The Astrophysical Journal, 910:107 (7pp), 2021 April 1 https://doi.org/10.3847/1538-4357/abe62c

Backstreaming Pickup Ions

Michael Gedalin[1], Nikolai V. Pogorelov[2,3], and Vadim Roytershteyn[4]
[1] Department of Physics, Ben Gurion University of the Negev, Beer-Sheva, Israel; gedalin@bgu.ac.il
[2] Department of Space Science, The University of Alabama in Huntsville, AL 35805, USA
[3] Center for Space Plasma and Aeronomic Research, The University of Alabama in Huntsville, AL 35805, USA
[4] Space Science Institute, Boulder, CO 80301, USA
Received 2020 November 22; revised 2021 February 10; accepted 2021 February 11; published 2021 April 2

Abstract

Ions that are reflected at the shock front and escape back into the upstream region can play the role of ions that start to be accelerated by a diffusive shock acceleration mechanism. Backstreaming ions have been shown to be generated from a superthermal tail of the solar wind at sufficiently high upstream temperatures. The number of such ions was found to be low and they were not found at shock angles exceeding 50°. The mechanism of production is multiple reflection when an ion changes the direction of motion inside the ramp for the first time, due to the cross-shock potential. Since pickup ions (PUIs) constitute a strongly superthermal population of protons a substantially stronger production of backstreaming PUIs can be expected. We study the reflection of PUIs in a planar stationary shock front using test particle analysis. The used model is inspired by the observed profile of the termination shock. The influence of magnetic compression, the shock angle, and the overshoot are analyzed. It is found that generation of backstreaming PUIs in this shock is substantially more efficient than the generation of backstreaming protons from thermal solar wind. The fraction of backstreaming PUIs rapidly increases with the increase of magnetic compression and the decrease of the shock angle. Overshoot enhances production of backstreaming PUIs and allows it for larger shock angles. No backstreaming ions have been found for shock angles larger than 60°. The results of the test particle analysis are supported by full-particle simulations.

Unified Astronomy Thesaurus concepts: Shocks (2086); Termination shock (1690); Interplanetary particle acceleration (826)

1. Introduction

Collisionless shocks are widely believed to be one of the most efficient accelerators of charged particles in the universe. High energies are achieved via diffusive shock acceleration (Axford et al. 1977; Krymskii 1977; Bell 1978; Blandford & Ostriker 1978; Vasilev et al. 1978; Toptyghin 1980; Jokipii 1982; Drury 1983). However, the very beginning of this process Requires the generation of ions that propagate backwards in the upstream region. Such backstreaming is a prerequisite for any injection mechanism (Malkov & Voelk 1995; Scholer et al. 1998; Scholer & Kucharek 1998; Giacalone & Ellison 2000; Rice et al. 2000a; Rice et al. 2000b; Zank et al. 2001; Giacalone 2005). On the other hand, beams of ions propagating against the flow may be an important source of instabilities, which cause turbulence required for the scattering of accelerated ions. Production of backstreaming ions should be a part of the ion reflection at the shock front. Since different terminology is used by different researchers, to avoid confusion we clarify ours as follows: (a) directly transmitted ions cross the shock front once and proceed into the downstream region; (b) reflected–transmitted ions cross the shock more than once after which they proceed into the downstream region; and (c) backstreaming ions cross the shock front more than once after which they escape into the upstream without returning further to the shock and no additional diffusive mechanism is involved. Reflected–transmitted and backstreaming ions are often referred to together as reflected ions, although the fate of these two populations is quite different. It is backstreaming ions that can play the role of the superthermal population injected into the diffusive shock acceleration process. Observations at the Earth's bow shock have revealed populations of backstreaming ions persistent well ahead of the shock and apparently related to the magnetic field fluctuations (Meziane et al. 2004). Generation of these populations by shocks is not well understood at present. Numerical simulations (Burgess 1987) and theory (Gedalin et al. 2008; Gedalin 2016) do not show backstreaming ions for the angle between the shock normal and the upstream magnetic field $\theta_{\rm Bn} > 60°$. Yet, observations have revealed such ions in nearly perpendicular shocks (Kucharek et al. 2004; Oka et al. 2005). It has been shown (Gedalin 2016) that efficiency of the backstreaming ion production rapidly increases with the increase of the ratio v_T/V_u, where v_T is the thermal speed of the incident ions and V_u is the upstream flow velocity along the shock normal in the shock frame. The latter is the same as the shock speed in the upstream fluid frame. Thus, one can expect that backstreaming ions would be more efficiently produced if the upstream ion distribution contained a substantial superthermal population (Chalov 2000, 2019; Burrows et al. 2010; Zank et al. 2014; Chalov et al. 2016). Pickup ions (PUIs) may well play the role of such populations since they have typical thermal speeds $v_T \approx V_u$ (Vasyliunas & Siscoe 1976). In the outer heliosphere beyond ∼30 au the fraction of PUIs becomes substantial (Richardson & Stone 2009), so their contribution to the backstreaming ion beams may become dominant. The present research is aimed to analyze the dependence of the number and distribution of backstreaming PUIs on the basic shock parameters.

2. The Shock Model

Since the PUI dynamics in the shock front are nonadiabatic and the equations of motion are not integrable, we resort to test particle analysis in a model shock front. This approach proved to be efficient in the determination of dependencies, although

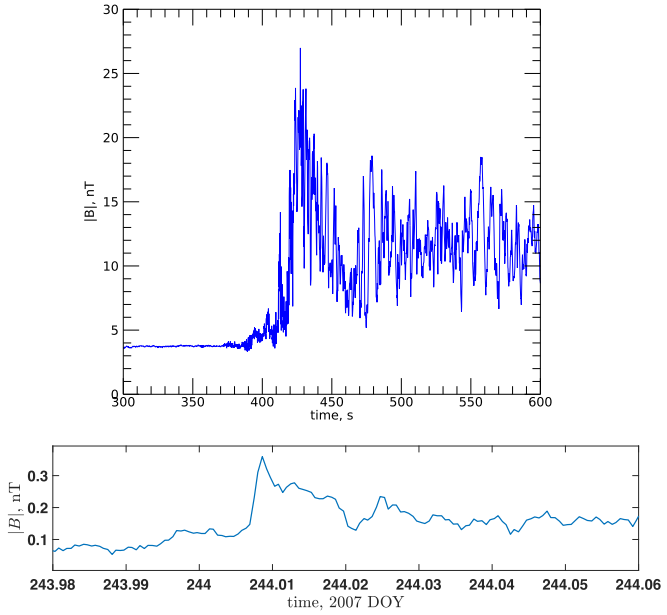

Figure 1. Top panel: an example of the MMS observed terrestrial bow shock. Bottom panel: the Voyager 2 observed termination shock.

the shock model is not self-consistent (Gedalin 1996, 2016; Gedalin et al. 2008, 2016, 2020; Gedalin & Dröge 2013). We assume that a planar stationary shock profile has been established due to the interaction of electromagnetic fields with charged particles and proceed by tracing the trajectories of ions in these steady fields. The shock normal is directed along the x-axis, from upstream to downstream. The noncoplanarity direction is along the y-axis, so that the shock transition is characterized by the jump in the component B_z.

The objectives of the present analysis are to find the dependence of the fraction of backstreaming ions on the shock angle θ_u, magnetic compression B_d/B_u, and cross-shock potential (see below). Because of the presence of a substantial fraction of PUIs, more than 10%, the magnetic compression for a given Alfvénic Mach number is lower than it would be without PUIs (Burlaga et al. 2008; Richardson et al. 2008; Gedalin et al. 2020). The top panel of Figure 1 shows an example of the terrestrial bow shock observed by the Multi-scale Magnetospheric (MMS) mission on 2018 October 25, at around 08:00. The data were retrieved using the Spedas software from the publicly available database. The bottom panel shows, for comparison, the termination shock observed by Voyager 2 on 2007 September 1. The data were retrieved from the publicly available server[5]. The main features of the profiles exploited in this paper are a sharp increase in the magnetic field strength (ramp) followed by a large overshoot, where the magnetic field substantially exceeds the downstream magnetic field. Behind the overshoot, the magnetic field drops down to the downstream value or below it at a scale noticeably larger than the ramp width. The terrestrial bow shock is much better resolved, and the ramp looks structured and probably nonstationary. The ramp of the termination shock also shows some internal structure or nonstationarity not shown here (Burlaga et al. 2008). Ion dynamics in the shock front depend substantially on v_T/V_u, where v_T is the upstream thermal velocity of the ion population (Gedalin 1996, 2016; Gedalin et al. 2008; Gedalin & Dröge 2013). For PUIs, this ratio is $v_T/V_u \sim 1$. Therefore, the Alfvénic Mach number $M_A = V_u/v_A$ is relevant only for the shock width, which is taken on the order of the ion inertial length c/ω_{pi} and is by the factor of $1/M_A$ smaller than the proton convective gyroradius V_u/Ω_u. Here $\Omega_u = eB_u/m_pc$ is the upstream proton gyrofrequency, $\omega_{pi} = \sqrt{4\pi n_u e^2/m_p}$ is the upstream proton plasma frequency, and $v_A = c\Omega_u/\omega_{pi}$. The above parameters refer to the solar wind protons only and do not include PUIs. For $M_A \gtrsim 3$ the ramp width is sufficiently small in relation to the convective gyroradius to cause significant magnetic deflection of the bulk flow (Gedalin 1996, 1997, 2020). In the presented analysis, the Mach numbers are chosen close to the estimated Mach numbers at the termination shock (Burlaga et al. 2008; Richardson et al. 2008), within the range $5 < M_A < 7$. For these Mach numbers, the shock profiles of the terrestrial bow shock (Scudder et al. 1986; without PUIs) and the termination shock (Burlaga et al. 2008; with the PUI presence being substantial) are similar and differ mainly in the strength of the overshoot and downstream magnetic compression, which are lower for the PUI-affected termination shock. The parameters used here are appropriate when the contribution of PUIs is significant and are consistent with full particle simulations (see below). Ion tracing is performed in the de Hoffmann–Teller (HT) frame, where the upstream plasma flow is along the magnetic field $\boldsymbol{V}_{HT,u} = (V_u, 0, V_u \tan\theta_u)$ and there is no motional electric field $E_y = E_z = 0$ throughout. There is a nonzero E_x inside the shock transition layer. This electric field is directed against the incident ion flow. The model electric field shape is chosen as $E_x \propto dB_z/dx$ with the cross-shock potential $\phi_{HT} = -\int E_x dx$ as a model parameter. The noncoplanar magnetic field is chosen as $B_y \propto E_x$ and

$$(V_u \tan\theta_u/c) \int B_y dx = (\phi_{NIF} - \phi_{HT}) \quad (1)$$

where ϕ_{NIF} is the cross-shock potential in the normal incidence frame (NIF). The NIF is the frame in which the upstream plasma flow is along the shock normal. It has been shown that ϕ_{NIF} may affect the ion motion significantly, whereas ϕ_{HT} is of almost no importance (Gedalin 2016, 2020; Gedalin et al. 2020). In what follows, we keep $e\phi_{HT} = 0.1(m_pV_u^2/2)$ while ϕ_{NIF} is varied.

3. PUI Tracing

The upstream distribution of 80,000 ions is chosen in the form of a filled shell (Vasyliunas & Siscoe 1976), i.e., $f_u(\boldsymbol{u}) \propto u^{-3/2}H(u_c - u)$, where $u = \sqrt{(v_x - V_u)^2 + v_y^2 + (v_z - V_u\tan\theta_u)^2}$ is the velocity of PUIs in the solar wind frame, u_c is the cutoff speed, and H is the Heaviside step function. A low-speed cutoff is applied to avoid numerical divergences. In the presented test particle analysis, $u_c = V_u$. For the monotonic profiles below, the Mach number is $M_A = 5.5$. The results of the tracing are presented for $\theta_u = 65°$, 60°, 55°, 50°, 45°, and $B_d/B_u = 2$, 2.2, 2.5. In all these runs, $e\phi_{NIF} = 0.35(m_pV_u^2/2)$ (low potential). No backstreaming ions were found for $\theta_u = 65°$ or $\theta_u = 60°$.

For $B_d/B_u = 2$, we also analyzed $e\phi_{NIF} = 0.55(m_pV_u^2/2)$ (high potential). No backstreaming ions were found for $\theta_u = 65°$ or $\theta_u = 60°$. Figure 2 illustrates the upstream and downstream gyrophase averaged distributions $v_\perp f(v_\parallel, v_\perp)$ in the case $\theta_u = 60°$, $B_d/B_u = 2.5$, and for the low potential. Here

[5] https://spdf.gsfc.nasa.gov/pub/data/voyager/voyager2/magnetic_fields/

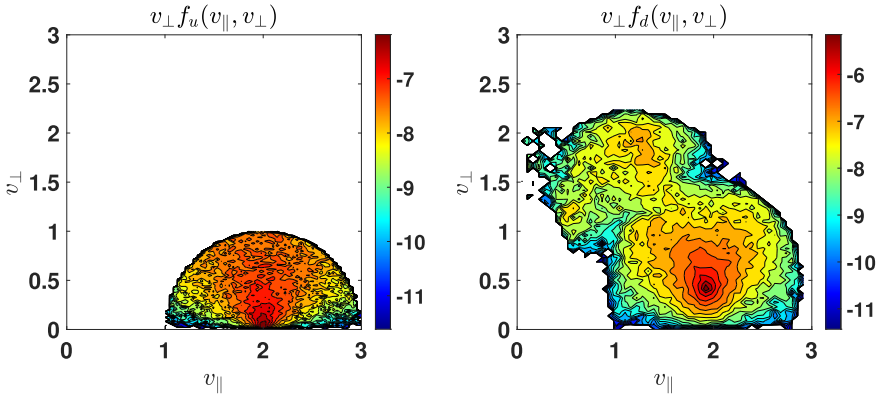

Figure 2. Upstream (left) and downstream (right) $v_\perp f(v_\parallel, v_\perp)$ of PUIs for $\theta_u = 60°$, $B_d/B_u = 2.5$, and low potential (logarithmic scale). The velocities are normalized on V_u.

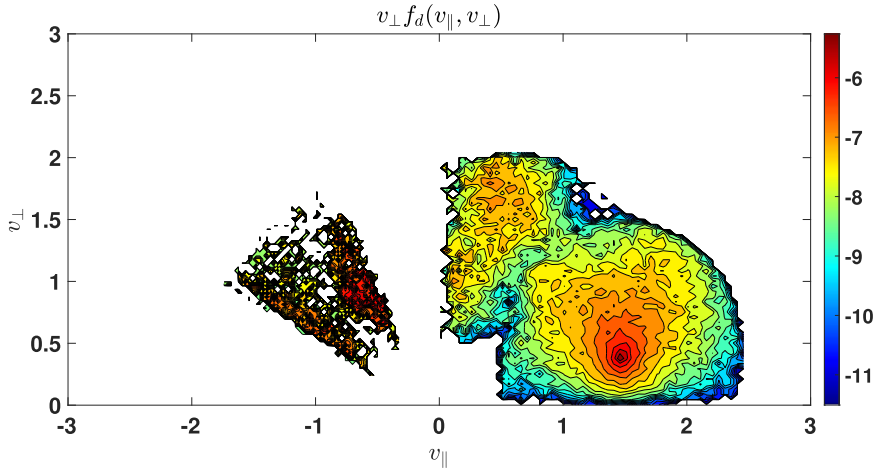

Figure 3. Distributions of backstreaming (left) and downstream (right) PUIs for $\theta_u = 50°$, $B_d/B_u = 2.2$, and low potential (logarithmic scale).

$v_\parallel = |\boldsymbol{v}\cdot\boldsymbol{B}|/|\boldsymbol{B}|$ and $v_\perp = \sqrt{v^2 - v_\parallel^2}$, while $\boldsymbol{B}$ is the downstream magnetic field for the transmitted ions and the upstream magnetic field for the incident and backstreaming ions. The velocities are normalized to V_u. The parallel and perpendicular directions are chosen with respect to the local magnetic field direction. The contour is shown in the logarithmic scale. The initial upstream distribution is the same for all runs. The downstream distribution clearly shows directly transmitted ions and singly reflected ions. This structure is quite typical (Gedalin et al. 2020).

Figure 3 shows the distributions of backstreaming and downstream PUIs (calculated separately) in the same format as in Figure 2. In this case, we choose $\theta_u = 50°$, $B_d/B_u = 2.2$, and low potential $e\phi_{\rm NIF} = 0.35(m_p V_u^2/2)$. The backstreaming ions are gyrating around the magnetic field $v_\perp \neq 0$. This is illustrated by Figure 4, where the upstream, downstream, and backstreaming ions are shown as points in the velocity space $(v_{\perp,1}, v_{\perp,2}, v_\parallel)$. Here the subscript $\perp$, 2 refers to the direction along the y-axis, while the subscript $\perp$, 1 is for the direction perpendicular to both the magnetic field and y-axis. The downstream and backstreaming ions are caught at the positions $8(V_u/\Omega_u)$ and $-10.5(V_u/\Omega_u)$ and therefore are not gyrophase averaged.

Table 1 gives the fraction of backstreaming ions. The fraction rapidly increases with the decrease of the angle and increase of the magnetic compression. A higher cross-shock potential also enhances generation of backstreaming ions. It

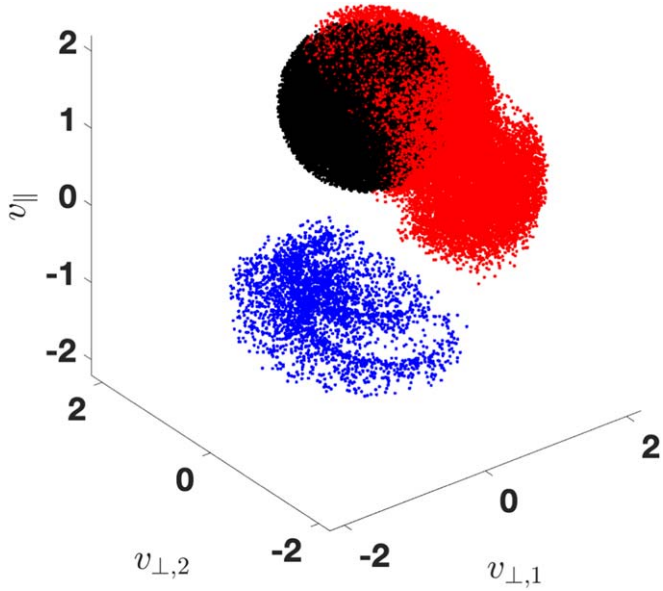

Figure 4. Upstream (black), downstream (red), and backstreaming (blue) PUIs shown as points in the velocity space $(v_{\perp,1}, v_{\perp,2}, v_\parallel)$, for $\theta_u = 50°$, $B_d/B_u = 2.2$, and low potential (logarithmic scale).

should be remembered, however, that the cross-shock potential cannot be too large and is smaller for higher Mach numbers (Gedalin & Balikhin 2004). As expected, the fraction of

Table 1
Fraction of Backstreaming Ions (%)

B_d/B_u θ	2	2.2	2.5	2 (High Potential)
55°	0.21	0.87	2.57	0.74
50°	2.45	4.	7.36	3.92
45°	5.9	8.37	12.83	10.6

backstreaming PUIs is substantially larger than that for thermal protons (Gedalin et al. 2008). However, the mechanism of reflection is somewhat different. A typical trajectory of a backstreaming PUI in a shock without overshoot is shown in Figure 5 as the dependence of the v_x component of the velocity on the coordinate along the shock normal. The ion crosses the ramp completely and turns back for the first time in the uniform downstream magnetic field. The majority of backstreaming ions in this shock overcome the cross-shock potential barrier and experience multiple reflection. In previous studies of the generation of backstreaming population from the thermal distribution of the solar wind (Gedalin et al. 2008; Gedalin 2016) it was found that such ions are turned back inside the ramp by the electrostatic potential, which is followed by an additional loop, or several loops, around the ramp, after which the ion finally escapes into the upstream region and does not return to the shock any longer.

4. Overshoot Influence

At Mach numbers $M > 3$ a noticeable overshoot is expected to be present at the downstream side of the magnetic profile, and the overshoot strength increases as the Mach number increases (Greenstadt et al. 1980; Russell et al. 1982; Mellott & Livesey 1987). We study the effect of the overshoot by modifying the shock profile. The main component of the magnetic field B_z is modeled as follows:

$$B_1 = \left(\frac{R+1}{2}\right) + \left(\frac{R-1}{2}\right)\tanh\left(\frac{ax}{D}\right) \quad (2)$$

$$f_l = \frac{1}{2}\left[1 + \tanh\left(\frac{x - C_l}{W_l}\right)\right] \quad (3)$$

$$f_r = \frac{1}{2}\left[1 - \tanh\left(\frac{x - C_r}{W_r}\right)\right] \quad (4)$$

$$B_z = (B_1 + B_o f_1 f_2) B_u \sin\theta_u. \quad (5)$$

In the present paper, the following parameters are used: $a = 3$, $D = (c/\omega_{\rm pi})$, $W_l = (c/\omega_{\rm pi})$, $W_r = 1.5(c/\omega_{\rm pi})$, and $C_l = C_r = 0$. The main magnetic compression R is related to B_d/B_u as follows:

$$\frac{B_d}{B_u} = \sqrt{R^2 \sin^2\theta_u + \cos^2\theta_u}. \quad (6)$$

An example of such a profile is shown in Figure 6 (to be compared with Figure 1). The cross-shock potential has to be reduced, since $\phi_{\rm max} = (B_{\rm max}/B_d)\phi_{\rm NIF}$, and there is an excessively high potential at the overshoot, which may cause unphysically strong ion reflection. Therefore, for the overshoot studies we use $e\phi_{\rm NIF} = 0.25(m_p V_u^2/2)$ to keep $\phi_{\rm max}$ approximately consistent with the values that were used without an overshoot. In what follows $M = 6.5$ and $\theta = 60°$. Figure 7 shows orbits of two backstreaming PUIs for $B_{\rm max}/B_u \approx 4$.

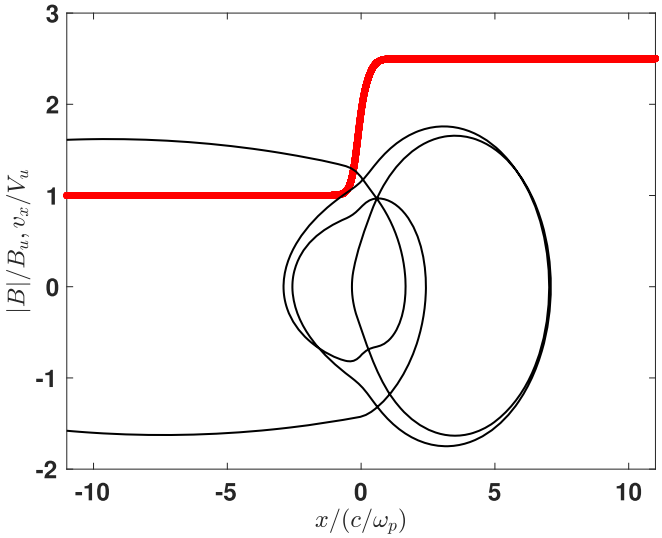

Figure 5. A typical trajectory, $x - v_x$, of a backstreaming PUI without overshoot. The magnetic profile is in red.

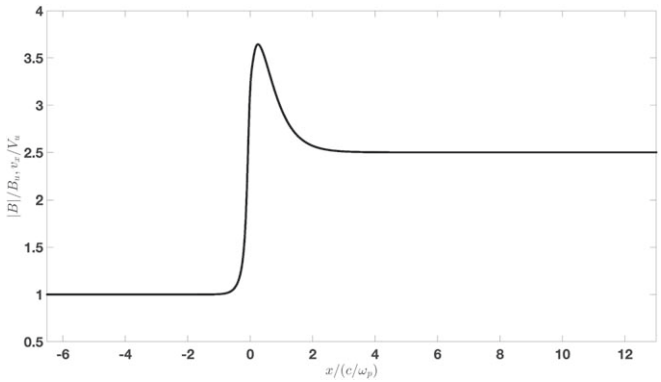

Figure 6. An example of the magnetic profile with an overshoot.

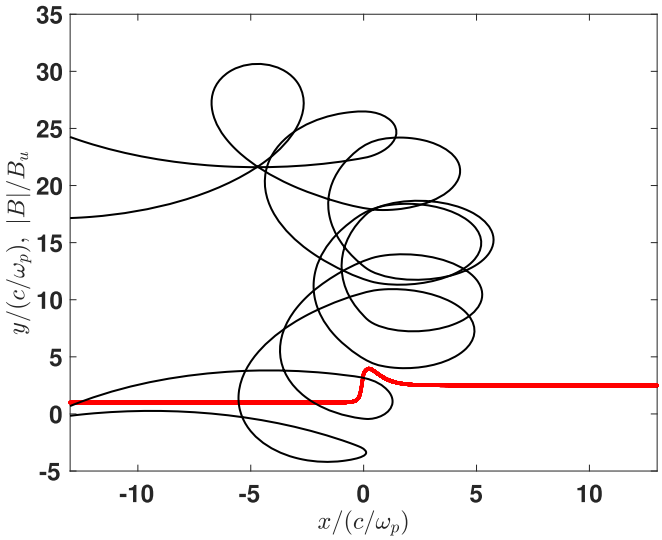

Figure 7. Orbits of backstreaming ions for $B_d/B_u = 2.5$, $\theta = 60°$, $M = 6.5$, $e\phi_{\rm NIF} = 0.25(m_p V_u^2/2)$, and $B_{\rm max}/B_u \approx 4$.

Depending on the initial velocity at the upstream edge of the ramp, two reflection regimes are possible (Gedalin 2016): (a) an ion having a low v_x can be stopped and turned back inside the ramp, mainly by the cross-shock potential, and (b) an ion

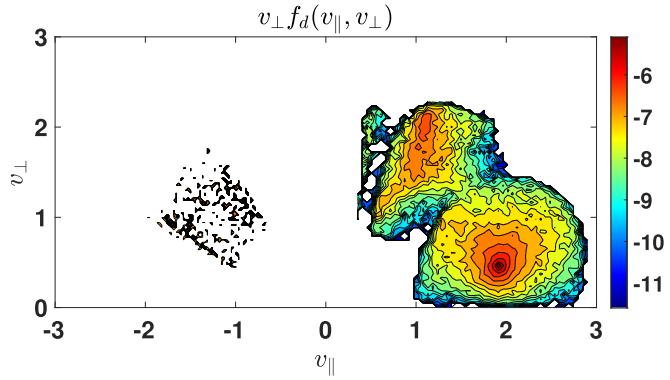

Figure 8. PUI distribution upon scattering at the shock front for $B_d/B_u = 2.5$, $\theta = 60°$, $M = 6.5$, $e\phi_{\rm NIF} = 0.25(m_p V_u^2/2)$, and $B_{\rm max}/B_u \approx 4$.

with a high v_x can gyrate back to the ramp after crossing it once. It has been shown that backstreaming ions coming from the thermal solar wind distribution are produced via the first kind of reflection, which is followed by additional loops around the ramp (Gedalin et al. 2008; Gedalin 2016). PUIs are significantly superthermal and one can expect that the second regime would play an important role in this case. Indeed, Figure 7 shows that both kinds of reflection are present: one ion crosses the ramp and comes back, another one returns inside the ramp. The fraction of backstreaming PUIs is ≈1%. These ions are barely seen in the contour plot in Figure 8. When the overshoot is reduced to $B_{\rm max}/B_u \approx 3$ there are still backstreaming PUIs but the fraction drops to ≈0.25%.

5. Full-particle Simulations

A series of one-dimensional particle-in-cell (PIC) simulations have been performed. The shock was formed by reflection off a wall at one side of the simulation box, while a three-component plasma (electrons, solar wind protons, and PUIs) with fixed upstream distributions was injected from another. The simulations were performed using the Vector Particle-In-Cell (VPIC) code (Bowers et al. 2008). The simulation discussed here had the following parameter: the domain size was $L = 200(c/\omega_{\rm pi})$ with 178,688 cells. The mass ratio between protons and electrons was $m_p/m_e = 400$ and the Alfvén speed was $V_{\rm A}/c = 0.005$. Here c is the speed of light. We present only the case with $\theta_u = 60°$. The upstream electron and SW protons were Maxwellian, with the temperature corresponding to $\beta_e = \beta_{p,\rm SW} = 0.1$. The PUIs had the same filled shell distribution used in the above ion tracing, with the cutoff speed $u_c = 7V_{\rm A}$. The upstream PUIs' density was 20% of the total. The upstream plasma is represented by 1000 electrons, 750 solar wind protons, and 250 PUIs per cell. The injection speed of the upstream plasma was $4.5V_{\rm A}$. The shock speed in the simulation frame was about $2.2V_{\rm A}$, which means that $M_{\rm A} \approx 6.7$. Note that the cutoff speed u_x slightly exceeds the shock speed V_u. Figure 9 shows the components of the magnetic field at the stage when the shock is already fully developed. While the shock is not completely independent of time, the main features of the magnetic profile are quite stable and similar to the adopted model, so it is reasonable to compare ion dynamics with ion tracing in a model shock. Figure 10 illustrates the appearance of a small number (approximately 3.5%) of backstreaming PUIs in the upstream region using a snapshot of the distribution in the plane perpendicular to the shock

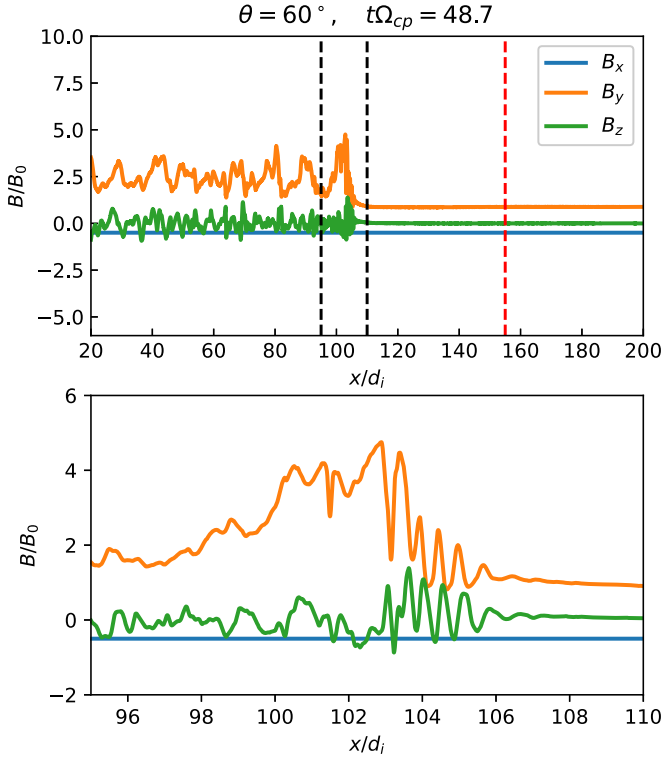

Figure 9. Top: magnetic field of the PIC-simulated shock described in the text. The red dashed line shows the location where distribution functions are collected (see Figure 10 below). The bottom panel shows an expanded view of the transition region, marked by two black vertical dashed lines in the top panel.

normal for $\theta_u = 60°$ (left panel). The PIC distribution function is shown in the NIF and the format of the presentation differs from that for ion tracing. Yet, the backstreaming PUI population is clearly seen, although the density is low. There are no backstreaming PUIs for $\theta_u = 70°$ (right panel). No backstreaming solar wind protons are present in either case.

6. Conclusions

We have studied the generation of backstreaming PUIs in a one-dimensional stationary shock front with and without overshoot. The model shock profile, used for ion tracing as test particles, was chosen to closely resemble the observed termination shock profile and the one found in our PIC simulations. The main objective was to quantify the effects of the major stationary planar features of the ramp and overshoot. Therefore, time dependence or deviations from planarity were not taken into account, and the study was limited to the quasi-perpendicular regime $\theta_u > 50°$, where the effects of time dependence and deviations from planarity are expected to be weak. The analysis has revealed that the downstream distributions of PUIs have similar patterns in a wide range of shock angles for modest magnetic compression ratios. The number of backstreaming ions rapidly increases with the decrease of the shock angle. Larger magnetic compressions also result in a larger fraction of backstreaming PUIs. We have not found backstreaming PUIs for $\theta_u > 55°$ if the overshoot is absent. Substantial overshoots result in small fractions of backstreaming PUIs for $\theta_u = 60°$ too. Yet, at larger angles, no backstreaming ions are generated. For all quasi-perpendicular

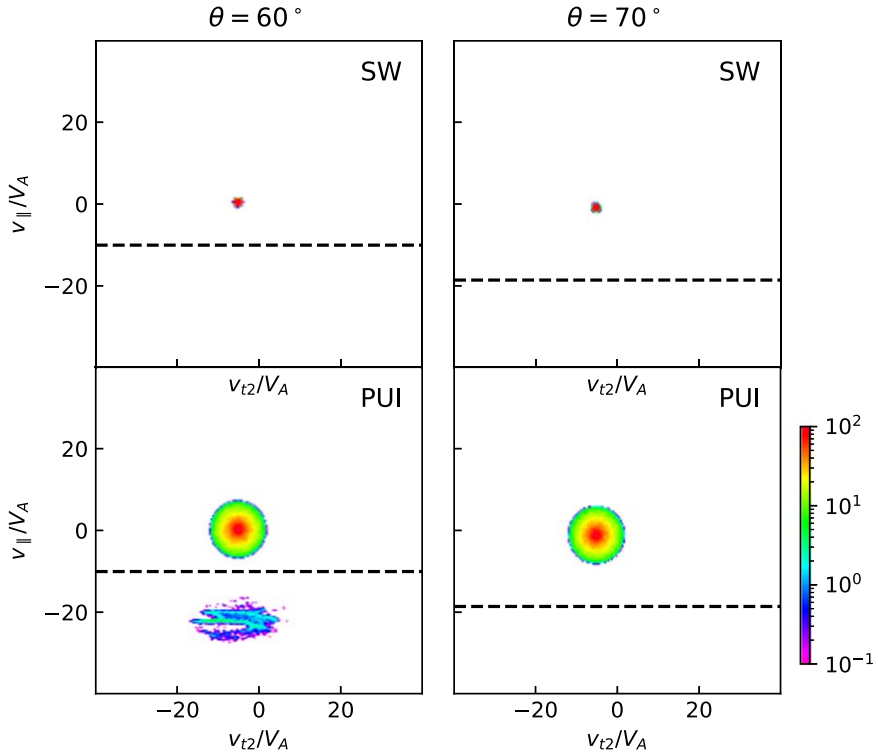

Figure 10. An upstream snapshot of solar wind and PUI distributions (particle counts) for solar wind protons (top) and PUIs (bottom). Here $\boldsymbol{t}_2$ is a unit vector in the direction of $\boldsymbol{B}_0 \times (\boldsymbol{n} \times \boldsymbol{B}_0)$. Left panel: backstreaming PUIs for $\theta_u = 60°$. Right panel: no backstreaming ions for $\theta_u = 67°$.

cases the fraction of backstreaming PUIs is very low and their effect on the upstream pressure is negligible. Yet, even at these low fluxes, backstreaming PUIs may cause instabilities. This subject is beyond the scope of the present paper. At present there is no sufficient observational data to compare with. If backstreaming ions are present for higher obliquities, the mechanism of their generation may be related to the shock nonplanarity or time dependence. Nonstationary and/or nonplanar features are expected to affect PUI dynamics at the lower θ_u. These issues will be studied separately with test particle analyses in nonplanar (rippled) shock fronts and 2D PIC simulations.

This research was partially supported by NASA grant 80NSSC18K1649NS and NSF-BSF grants 2010144 and 2010450. N.P. was also supported by the IBEX mission as a part of NASA's Explorer program. The authors acknowledge the Texas Advanced Computing Center (TACC) at The University of Texas at Austin for providing HPC resources on Frontera supported by NSF LRAC award 2031611, which have contributed to the research results reported within this paper. PIC simulations were partly performed using resources provided by the NASA High-End Computing (HEC) Program through the NASA Advanced Supercomputing (NAS) Division at Ames Research Center. M.G. was partially supported by NSF-BSF grant 2019744.

ORCID iDs

Michael Gedalin https://orcid.org/0000-0003-1236-4787
Nikolai V. Pogorelov https://orcid.org/0000-0002-6409-2392
Vadim Roytershteyn https://orcid.org/0000-0003-1745-7587

References

Axford, W. I., Leer, E., & Skadron, G. 1977, ICRC (Plovdiv), 11, 132
Bell, A. R. 1978, MNRAS, 182, 147
Blandford, R. D., & Ostriker, J. P. 1978, ApJ, 221, L29
Bowers, K. J., Albright, B. J., Yin, L., Bergen, B., & Kwan, T. J. T. 2008, PhPl, 15, 055703
Burgess, D. 1987, AnGeo, 5, 133
Burlaga, L. F., Ness, N. F., Acuña, M. H., et al. 2008, Natur, 454, 75
Burrows, R. H., Zank, G. P., Webb, G. M., Burlaga, L. F., & Ness, N. F. 2010, ApJ, 715, 1109
Chalov, S. V. 2000, Ap&SS, 274, 25
Chalov, S. V. 2019, Ap&SS, 364, 175
Chalov, S. V., Malama, Y. G., Alexashov, D. B., & Izmodenov, V. V. 2016, MNRAS, 455, 431
Drury, L. O. 1983, RPPh, 46, 973
Gedalin, M. 1996, JGR, 101, 4871
Gedalin, M. 1997, GeoRL, 24, 2511
Gedalin, M. 2016, JGRA, 121, 10754
Gedalin, M. 2020, ApJ, 895, 59
Gedalin, M., & Balikhin, M. 2004, JGRA, 109, 3106
Gedalin, M., & Dröge, W. 2013, FrP, 1, 29
Gedalin, M., Dröge, W., & Kartavykh, Y. Y. 2016, ApJ, 825, 149
Gedalin, M., Liverts, M., & Balikhin, M. A. 2008, JGRA, 113, 05101
Gedalin, M., Pogorelov, N. V., & Roytershteyn, V. 2020, ApJ, 889, 116
Giacalone, J. 2005, ApJ, 628, L37
Giacalone, J., & Ellison, D. C. 2000, JGR, 105, 12541
Greenstadt, E. W., Scarf, F. L., Russell, C. T., et al. 1980, JGR, 85, 2124
Jokipii, J. R. 1982, ApJ, 255, 716
Krymskii, G. F. 1977, SPhD, 22, 327
Kucharek, H., Möbius, E., Scholer, M., et al. 2004, AnGeo, 22, 2301
Malkov, M., & Voelk, H. 1995, A&A, 300, 605
Mellott, M. M., & Livesey, W. A. 1987, JGR, 92, 13661
Meziane, K., Wilber, M., & Mazelle, C. 2004, JGRA, 109, A05107
Oka, M., Terasawa, T., Saito, Y., & Mukai, T. 2005, JGRA, 110, A05101
Rice, W., Zank, G., & Le Roux, J. 2000a, GeoRL, 27, 3793
Rice, W. K. M., Zank, G. P., Richardson, J. D., & Decker, R. B. 2000b, GeoRL, 27, 509
Richardson, J. D., Kasper, J. C., Wang, C., Belcher, J. W., & Lazarus, A. J. 2008, Natur, 454, 63

Richardson, J. D., & Stone, E. C. 2009, SSRv, 143, 7
Russell, C. T., Hoppe, M. M., & Livesey, W. A. 1982, Natur, 296, 45
Scholer, M., & Kucharek, H. 1998, Ap&SS, 264, 527
Scholer, M., Kucharek, H., & Trattner, K. 1998, AdSpR, 4, 533
Scudder, J. D., Aggson, T. L., Mangeney, A., Lacombe, C., & Harvey, C. C. 1986, JGR, 91, 11019
Toptyghin, I. N. 1980, SSRv, 26, 157
Vasilev, V. N., Toptygin, I. N., & Chirkov, A. G. 1978, Ge&Ae, 18, 415
Vasyliunas, V. M., & Siscoe, G. L. 1976, JGR, 81, 1247
Zank, G., Rice, W., Le Roux, J., Cairns, I., & Webb, G. 2001, PhPl, 8, 4560
Zank, G. P., Hunana, P., Mostafavi, P., & Goldstein, M. L. 2014, ApJ, 797, 87